Title

Programming the Self-Organization of Endothelial Cells into Perfusable Microvasculature

Journal

Tissue Engineering Part A, 29(3-4)

ISSN

1937-3341

Authors

Cabral, Katelyn A
Srivastava, Vasudha
Graham, Austin J
et al.

Publication Date

2023-02-01

DOI

10.1089/ten.tea.2022.0072

Peer reviewed

TISSUE ENGINEERING: Part A
Volume 29, Numbers 3 and 4, 2023

DOI: 10.1089/ten.tea.2022.0072

termis
Tissue Engineering
& Regenerative Medicine
International Society

Open camera or QR reader and scan code to access this article and other resources online.

ORIGINAL ARTICLE

Programming the Self-Organization of Endothelial Cells into Perfusable Microvasculature

Katelyn A. Cabral, PhD,[1] Vasudha Srivastava, PhD,[2] Austin J. Graham, PhD,[2,5] Maxwell C. Coyle, BS,[3] Connor Stashko, PhD,[1] Valerie Weaver, PhD,[4] and Zev J. Gartner, PhD[2,5,6]

The construction of three-dimensional (3D) microvascular networks with defined structures remains challenging. Emerging bioprinting strategies provide a means of patterning endothelial cells (ECs) into the geometry of 3D microvascular networks, but the microenvironmental cues necessary to promote their self-organization into cohesive and perfusable microvessels are not well known. To this end, we reconstituted microvessel formation *in vitro* by patterning thin lines of closely packed ECs fully embedded within a 3D extracellular matrix (ECM) and observed how different microenvironmental parameters influenced EC behaviors and their self-organization into microvessels. We found that the inclusion of fibrillar matrices, such as collagen I, into the ECM positively influenced cell condensation into extended geometries such as cords. We also identified the presence of a high-molecular-weight protein(s) in fetal bovine serum that negatively influenced EC condensation. This component destabilized cord structure by promoting cell protrusions and destabilizing cell–cell adhesions. Endothelial cords cultured in the presence of fibrillar collagen and in the absence of this protein activity were able to polarize, lumenize, incorporate mural cells, and support fluid flow. These optimized conditions allowed for the construction of branched and perfusable microvascular networks directly from patterned cells in as little as 3 days. These findings reveal important design principles for future microvascular engineering efforts based on bioprinting and micropatterning techniques.

Keywords: engineered tissues, engineered microvasculature, bioprinting, cell patterning, optimization, cell behavior, microenvironment, tissue morphogenesis, vasculogenesis

Impact Statement

Bioprinting is a potential strategy to achieve microvascularization in engineered tissues. However, the controlled self-organization of patterned endothelial cells into perfusable microvasculature remains challenging. We used DNA Pro-

[1]Graduate Program in Bioengineering, University of California, San Francisco and University of California, Berkeley, Berkeley, California, USA.
[2]Department of Pharmaceutical Chemistry, University of California, San Francisco, San Francisco, California, USA.
[3]Department of Molecular and Cellular Biology, University of California, Berkeley, Berkeley, California, USA.
[4]Center for Bioengineering and Tissue Regeneration, Department of Surgery, University of California, San Francisco, San Francisco, California, USA.
[5]Chan Zuckerberg Biohub, University of California, San Francisco, San Francisco, California, USA.
[6]Center for Cellular Construction, University of California, San Francisco, San Francisco, California, USA.
This work was previously uploaded to Biorxiv (biorxiv.org) under the title ''Microenvironmental engineering improves the self-organization of patterned microvascular networks.'' doi: 10.1101/2022.04.04.487052

grammed Assembly of Cells to create cell-dense, capillary-sized cords of endothelial cells with complete control over their structure. We optimized the matrix and media conditions to promote self-organization and maturation of these endothelial cords into stable and perfusable microvascular networks.

Introduction

BIOENGINEERS CAN FACILITATE the ability of cells to self-organize into tissues by providing them with appropriate microenvironmental cues.[1–3] In the case of vasculature, many efforts have explored the microenvironmental cues that promote the formation of endothelial networks through a self-organizing process that mimics vasculogenesis.[4–6] Vasculogenesis typically begins with a randomly distributed population of cells and progresses through the coordination of a variety of distinct cell behaviors, including proliferation, mechanical polarization, motility, adhesion stabilization, and lumenization.[7] However, vasculogenesis (and self-organization in general) is also a highly stochastic process.[8] Consequently, the patterns of microvessels formed are challenging to control. By employing techniques such as bioprinting and microscale engineering, bioengineers can provide additional spatial cues to more deterministically guide self-organization.

These approaches reduce the subset of cell behaviors required to form mature microvessels, and thus limit the influence of stochastic processes on cell positioning.[6,9] Optimal deployment of these methods requires an understanding of the influence of each microenvironmental component on the cell behaviors necessary for each stage of endothelial cell (EC) self-organization.

Strategies for engineering microvasculature can be broadly categorized into bottom–up and top–down approaches.[9] Bottom–up approaches aim to engineer the self-organization processes of vasculogenesis and angiogenesis. When ECs are seeded within an extracellular matrix (ECM), they self-organize into microvascular networks with a broad distribution of network geometries and vessel diameters.[4,6,10,11] With application of interstitial fluid flow, these capillaries can lumenize and become perfused.[12–14] However, this process takes up to 7 days to complete due to the slow speed of angiogenesis (5 μm/hour)[15] and does not readily create hierarchical networks optimized for fluid transport.[16,17] Consequently, the center of thick and cell-dense tissues vascularized using these methods will suffer from hypoxia before completion of the process.[18,19] Top–down approaches, exemplified by bioprinting and microfabrication techniques, involve fabrication of hollow channels within hydrogels that are subsequently lined with a monolayer of ECs.[20–25]

This strategy excels at creating vascular structures that are hundreds of microns to millimeters in diameter with predefined geometry. However, the creation of capillary-sized vessels is challenging with top–down approaches due to the resolution limits of bioprinting and the tendency of narrow channels to clog when perfused with cell suspensions.[9,26]

Some bioprinting techniques allow for the rapid and direct placement of cells within ECMs at a high density, representing a potential hybrid approach.[3,27] Placing cells into a structure that resembles a vascular network effectively reduces the number of cell behaviors necessary to complete the process of self-organization and mitigates the effects of stochasticity. This potentially leads to more rapid vasculogenesis and better recapitulates more native-like and hierarchical vessel network geometries that are optimized for fluid flow.[28,29] For example, Brassard et al demonstrated the bioprinting of high-density cell solutions within Matrigel or collagen hydrogels.[3] Over time, the cells self-organized and condensed into a single cohesive structure in the geometry dictated by the initial print.

However, a limitation of this and other bioprinting techniques are the requirements on nozzle geometry and cell density, which effectively limit the diameter of the extruded close-packed and continuous vascular cords to around 250 μM—considerably larger than the diameter of capillaries. Consequently, no studies have yet reported on the microenvironmental cues required for narrow caliber, bioprinted vascular cords to self-organize into stable and perfusable networks.

To investigate the formation of microvessels <100 μm in diameter, we used DNA programmed assembly of cells (DPAC), a high-resolution cell patterning technique that allows for the formation of cell-dense tissues, fully embedded in a biologically relevant ECM, and with near single-cellular resolution in X and Y. We created capillary-sized lines of ECs within a three-dimensional (3D) ECM and observed their self-organization into microvessels under the influence of different microenvironmental cues. We found that by directly engineering the microenvironment, specific cell behaviors involved in latter stages of vasculogenesis can be encouraged, ultimately leading to the orderly self-organization of the cells into perfusable networks and across length scales that have not been previously achieved.

Method

Cell culture

Human umbilical vein ECs (HUVECs; Lonza) were cultured in EGM-2 and used between passages 4 and 6. Human brain vascular pericytes (HBVPs) were cultured in Dulbecco's modified Eagle's medium +10% fetal bovine serum (FBS) + penicillin/streptomycin and used between passages 4 and 13. Enhanced green fluorescent protein (EGFP)-HUVECs, EGFP-HBVPs, and mCherry-HUVECs were created by transducing cells with a pSicoR-EF1a-GFP or -mCherry lentivirus. HUVECs with cytosolic EGFP and nuclear mScarlet were created by transducing with a pSicoR-EF1a-EGFP-H2B-mScarlet lentivirus. All lentiviruses were made by the UCSF Viracore. Transduced cells were sorted on a BD Aria II flow cytometer.

Cell patterning

Cells were patterned using DPAC.[30–32] Briefly, aldehyde-functionalized glass slides (Nexterion) were micropatterned with amine-functionalized DNA oligonucleotides, either by spotting with a Nano eNabler (BioForce Nanosciences)[30,31]or by photolithography.[32,33] Reductive amination with 1% sodium borohydride resulted in a stable amine linkage between the oligonucleotides and the slide. The slide was treated with (tridecafluoro-1,1,2,2-tetrahydrooctyl) dimethylchlorosilane (Gelest) to render it hydrophobic and reduce nonspecific cell adhesion. Polydimethylsiloxane (PDMS) flow cells were plasma oxidized (Plasma Etch), placed atop the patterned slides, and treated with 1% bovine serum albumin (BSA) to further block nonspecific cell adhesion.

A cell suspension of HUVECs in serum-free EGM-2 was incubated with lipid- or cholesterol-modified oligonucleotide complexes complementary to the oligo patterned on the slide.[30–32] After washing to remove excess oligonucleotide, the cells were resuspended at a concentration of ~30 million cells/mL, added to the PDMS flow cells, and passed over the patterned slide. Washing out excess cells revealed selective adhesion of the cells to the DNA pattern. Multilayered endothelial cords were created by repeating this process with cells bearing oligonucleotides complementary to those in the previous layer.

A hydrogel precursor solution containing 2% Turbo DNase (Thermo Fisher Scientific) was added to the inlet of the PDMS flow cell and allowed to set around the patterned cells for 45 min at 37 °C. The cell-containing hydrogel was then carefully removed from the slide and placed atop a drop of liquid hydrogel precursor solution. This process fully embedded the two-dimensional-patterned cells into a 3D microenvironment. After 45 min of incubation at 37 °C, media were added and forceps was used to remove the PDMS flow cells from the hydrogel.

ECM hydrogel

Growth factor-reduced Matrigel (Corning) was mixed with 2% Turbo DNase and neutralized rat tail collagen I (Corning) for a total protein concentration of 8 mg/mL. The ratio of Matrigel to collagen varied by experiment. Nonspecific staining of the ECM was achieved by mixing the hydrogel precursor solution with 1% Alexa Fluor 647 NHS Ester (Invitrogen).

Media

Endothelial cords were cultured in EGM-2 (EBM-2 with the addition of EGM-2 BulletKit) (Lonza). For most experiments, 50 ng/mL phorbol-12-myristate-13-acetate (PMA) (Sigma-Aldrich) was added to the medium. For serum-free medium, the FBS was omitted from the EGM-2 (normally 2% of the volume). Recombinant human VEGF-A, FGF-basic, TGF-β1, stem cell factor (SCF), stromal cell-derived factor-1α (SDF-1α), and interleukin-3 (IL-3) were purchased from R&D Systems.

Multiple lots and formulations of FBS were evaluated, including FBS from EGM-2 Bulletkits (Lonza), UCSF Cell Culture Facility, and charcoal:dextran stripped FBS (Gemini Bio). Heat inactivation of FBS was achieved by heating to 56°C for 30 min. The FBS was fractionated by centrifuging through molecular weight cutoff filters (Sterlitech). The resulting concentrate and filtrate were then diluted with phosphate buffered saline (PBS) to the same volume as the FBS before filtration. To hydrolyze protein, 100 μg/mL of proteinase K (Fisher Scientific) was added to the FBS and then incubated at 55 °C for 1 h before being neutralized with 100 μg/mL phenylmethylsulfonyl fluoride (Millipore Sigma). Exosomes were purified from FBS using a Total Exosome Isolation Reagent Kit (Invitrogen).

Immunofluorescent staining

Tissues were fixed with 2% PFA for 45 min, permeabilized for 15 min with 1% Triton X-100 (Sigma-Aldrich) and blocked overnight with 10% goat serum. To avoid crossreactivity with the Matrigel, tissues that would later be treated with anti-mouse antibodies were also blocked with AffiniPure Fab Fragment Goat Anti-Mouse IgG (Jackson Laboratories). A list of antibodies used can be found in the Supplementary Methods.

Time-lapse microscopy

Patterned cell pairs were incubated for 12 h before being placed onto a Zeiss LSM800 microscope and imaged with a 25× objective every hour for 48 h. The cells were fed with media supplemented with 50 mM HEPES and ProLong Live Antifade Reagent (Thermo Fisher).

Image quantification

Cord morphology was quantified using FIJI.[34] The continuous length of each segment of cord was traced by hand (visualized by cytoplasmic EGFP). To further capture the scattering of the cords, the number of disconnected cells that had migrated away from the cord was manually counted and normalized per length of cord. Sprouts arising from the main cord were manually counted and normalized per length of the HUVEC cord. The number of protrusions per cell at 60 h of culture was counted manually. Cell protrusions were

FIG. 1. DPAC creates capillary-sized lines of HUVECs to assess the effect of ECM composition on EC self-organization. **(A)** Diagram of the cell patterning process. Amine-modified DNA oligos are selectively patterned onto aldehyde-functionalized glass slides and covalently bonded through reductive amination.[31,32] HUVECs are then labeled with a set of lipid- or cholesterol-modified complementary oligos that insert into the cell membrane. Upon passing the cells over the surface, the DNA hybridizes, adhering the HUVECs to the surface only in the regions defined by the DNA pattern. The HUVECs are then embedded in a hydrogel containing 2% DNase. After gelation, the hydrogel containing the patterned HUVECs is removed from the slide and placed on *top* of another droplet of hydrogel. The result is HUVECs that have been patterned with high precision in a single 2D plane but embedded within a 3D ECM. **(B)** Images of patterned HUVEC cords immediately after being fully embedded within the hydrogel. Scale bar: 500 μm. **(C)** Diagram showing the condensation of patterned HUVECs into either a single continuous structure or several smaller structures depending on matrix composition. **(D)** After 24 h of culture, patterned lines of HUVECs in MG broke up into several smaller, rounded sections (*top*). *Patterned lines* of HUVECs in MG-COL1 hydrogels were able to condense into a single cord structure (*bottom*). Scale bar: 100 μm. **(E)** The aspect ratio of cord segments cultured in MG-COL1 were significantly increased compared with MG alone (Mann-Whitney *U* test, $p < 0.0001$). Data were collected from three experiments, with 39 cords analyzed for MG and 54 cords analyzed from MG-COL1. Total number of segments analyzed: 216 for MG, 221 for MG-COL1. **(F)** HUVEC cords with fluorescent nuclei (H2B-mScarlet) and cytoplasm (EGFP) were cultured in either MG or MG-COL1 that had been stained with an Alexa Fluor 647 NHS-ester dye to visualize the ECM. ****$p < 0.0001$. 2D, two-dimensional; 3D, three-dimensional; DPAC, DNA programmed assembly of cells; EC, endothelial cell; ECM, extracellular matrix; EGFP, enhanced green fluorescent protein; HUVEC, human umbilical vein endothelial cell; COL1, collagen I; MG, Matrigel.

defined as extensions of the cytoplasm that were narrower than the nucleus and at least two microns in length. Pairs of cells were tracked manually at each hour of the 60-h time lapse and the number of instances in which the cells separated were recorded.

Statistics

All statistical analyses were performed using Prism 9. For analyses comparing two experimental conditions, an unpaired *t*-test was performed. For analyses comparing two experimental conditions, either an unpaired *t*-test or a Mann-Whitney *U* test was performed depending on whether the data was parametric or not.

Perfusion

Aluminosilicate glass micropipettes with a long tether were prepared using a P-97 micropipette puller (Sutter Instruments). The pulled pipettes were cut 3–5 mm from the tip to get 10–25 µm-diameter pipettes with jagged ends. The pipettes were filled with PBS or PBS containing 2 µm-

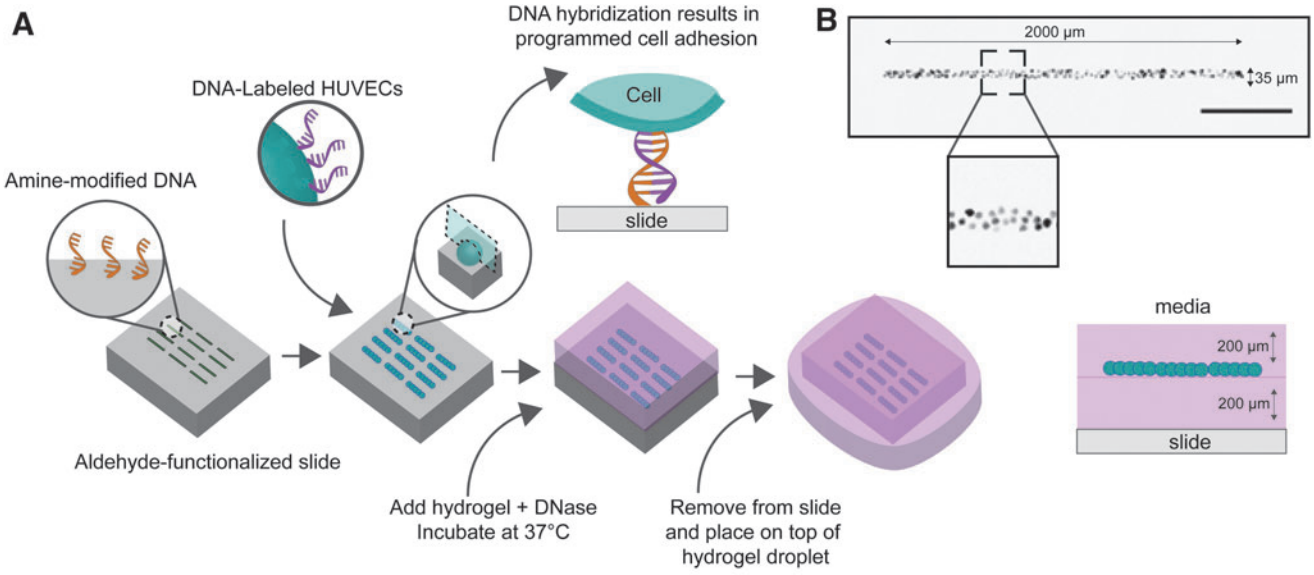

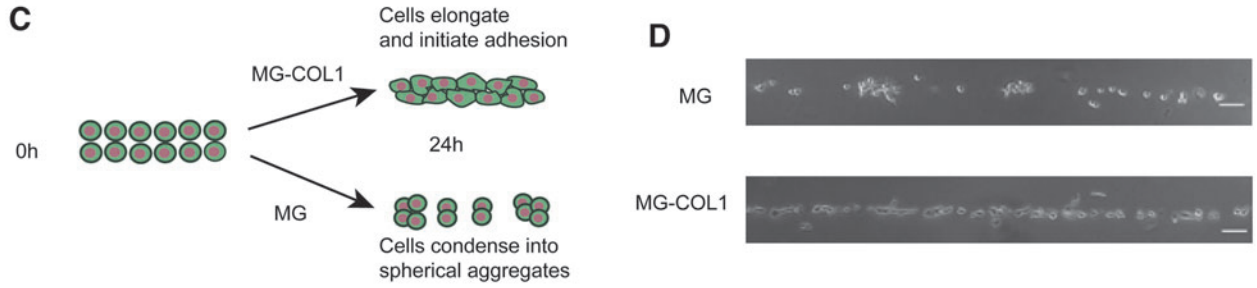

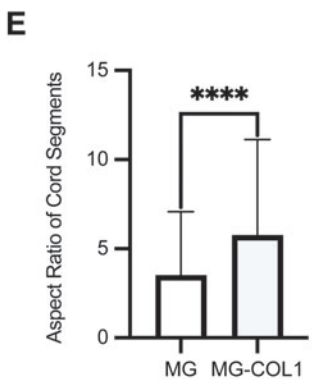

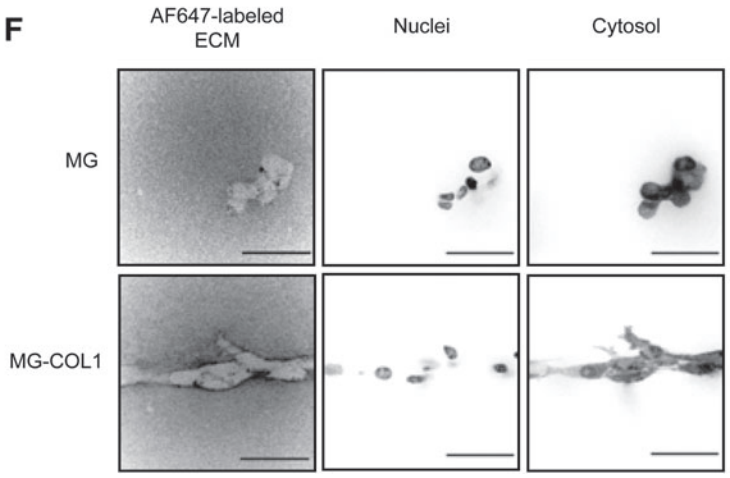

diameter FluoSpheres Carboxylate-Modified Microspheres (Thermo Fisher). The pipette was mounted on a Narishige MM-89 micromanipulator connected to a syringe. The endothelial cords were cut on one end to create an opening and the micropipette was used to puncture the opposite end of the cord. Once the tip of the micropipette was within the lumen of the cord, the syringe created a positive pressure and induced flow of liquid and debris toward the open end of the cord. Images were acquired using an Axiovert 200M epifluorescence microscope.

Endothelial barrier function

Rhodamine123 (Sigma-Aldrich), a cell-permeant small molecule dye, was injected into the lumen of endothelial cords by glass micropipette and images were taken of the dye and cords over the following 30 s. We measured the fluorescence intensity of the rhodamine123 and the mCherry-HUVECs across a ~10-μm-thick band through the cord. The fluorescence intensity of the rhodamine123 was compared with the predicted fluorescence intensity if there was no barrier function (i.e., free diffusion) using an analytical solution to Fick's Second Law, assuming an infinite concentration reservoir along the inner lumen walls, solved for various time points. In a separate experiment, Alexa Fluor 647-labeled BSA was added to the media and allowed to diffuse through the Matrigel (MG)–collagen I (COL1) hydrogel. After 21 min, the fluorescence intensity of the BSA and mCherry-HUVECs were measured across a ~30-μm-thick band through the endothelial cord. For both experiments, data were normalized by (Intensity–Minimum Intensity)/(Maximum Intensity–Minimum Intensity).

Experiment

We developed a reproducible assay to study the effect of microenvironmental cues on prepatterned ECs by constructing cell-dense, 35-μm-wide, 2-mm-long lines of HUVECs using DPAC (Fig. 1A).[30,32] DPAC allows for the placement of cells with single-cell precision in a common imaging plane and fully embedded within a 3D hydrogel. Using DPAC, we reproducibly patterned capillary-sized lines of ECs with an average nucleus-to-nucleus spacing of 25 μm, compared with ~15–21 μm nuclear spacing of capillaries *in vivo*[35] (Fig. 1B).

We first investigated components of the ECM microenvironment that promote the coalescence of micropatterned HUVECs into long multicellular cords (Fig. 1C). We narrowed our focus to combinations of basement membrane proteins (e.g., Matrigel) and stromal ECM (e.g., collagen I), as these conditions have been used to support the culture of organoids from a variety of tissues.[36–38] We found that EC lines cultured for 24 h in growth factor-reduced MG were mechanically unstable, fragmenting, and then condensing into several cell ''droplets'' (Fig. 1D). In contrast, identical EC lines cultured in a composite ECM of 6 mg/mL MG and 2 mg/mL COL1 (MG-COL1) were better able to maintain an extended morphology over 24 h. EC clusters were more elongated in MG-COL1 than MG, as evidenced by measuring the aspect ratio (Fig. 1E). Controlling for total protein concentration (8 mg/mL), we found that increasing the COL1 concentration in the hydrogel increased the length of the cord segments (Supplementary Fig. S1A).

We considered the possibility that COL1-containing gels increased endothelial spreading and angiogenic outgrowth due to elevated matrix stiffness.[39,40] However, there was no significant difference in the elastic modulus (E) between 8 mg/mL MG and MG-COL1 hydrogels, as measured by atomic force microscopy (Supplementary Fig. S1B) and bulk hydrogel rheology (Supplementary Fig. S1C). An alternative explanation stems from the ability of cells to mechanically remodel their microenvironment, including synthesizing ECM proteins, concentrating ECM components, and aligning them anisotropically.[41–43] We examined matrix remodeling using fluorescently labeled matrices. EC lines cultured in MG-COL1 gels concentrated ECM into bright sheaths at the cord surface, perhaps providing a more mechanically stable substrate to maintain an extended morphology (Fig. 1F).[42] The same was not true for EC lines cultured in Matrigel.

While collagen-containing hydrogels supported initial EC elongation into cord-like structures over 24 h (Fig. 2A), they failed to maintain this architecture and mature after

FIG. 2. Addition of PMA and removal of FBS results in stable, cohesive HUVEC cords with continuous adherens junctions. **(A)** Diagram showing that after the initial condensation of the patterned HUVECs into a single continuous structure, we need to find microenvironmental conditions to maintain that structure and stabilize the cord. **(B)** After 72 h of culture in EGM-2 media, HUVEC cords embedded in MG-COL1 scattered into small segments and individual cells. Scale bar = 100 μm. **(C)** The addition of 50 ng/mL PMA to the EGM-2 media resulted in somewhat more connected cords with many sprouts after 72 h. Scale bar = 100 μm. **(D)** After 72 h of culture in EGM-2 media without FBS, the HUVEC cords maintained one cohesive structure in the approximate shape of the original patterned vessel. Scale bar = 100 μm. **(E)** The percent of cords per tissue that had at least one segment longer than 500 μm in length at 72 h of culture in EGM-2 + PMA that either contained or omitted FBS. Bars represent mean ± SD and with each data point representing one independent tissue. Mann-Whitney *U* test, $p < 0.0001$. $n = 137$ cords across 13 tissues for EGM-2 + PMA + FBS and $n = 118$ cords for EGM-2 + PMA without FBS. **(F,** i) The number of disconnected cells that had migrated away from the cord per millimeter of HUVEC cords cultured for 72 h in either FBS-containing EGM-2 + PMA or FBS-free EGM-2 + PMA. Data represented as mean ± SD and with each data point representing one independent tissue. $n = 39$ cords cultured with FBS; 36 cords cultured without FBS. Mann-Whitney *U* test, $p < 0.0001$. (ii) The number of angiogenic sprouts per millimeter of HUVEC cords cultured for 72 h in either FBS-containing EGM-2 + PMA or FBS-free EGM-2 + PMA. Data represented as mean ± SD and with each data point representing one independent tissue. $n = 39$ cords cultured with FBS; 36 cords cultured without FBS. Mann-Whitney *U* test, $p < 0.0001$. **(G)** VE-cadherin staining in HUVEC cords cultured in either FBS-free EGM-2 + PMA or FBS-containing EGM-2 + PMA. Scale bar = 50 μm. **(H)** Comparison of HUVEC cords grown in either MG or MG-COL1, and in media containing or omitting FBS, after 72 h of culture. Scale bar: 100 μm. ****$p < 0.0001$. FBS, fetal bovine serum; PMA, phorbol-12-myristate-13-acetate; SD, standard deviation; VE, vascular endothelial.

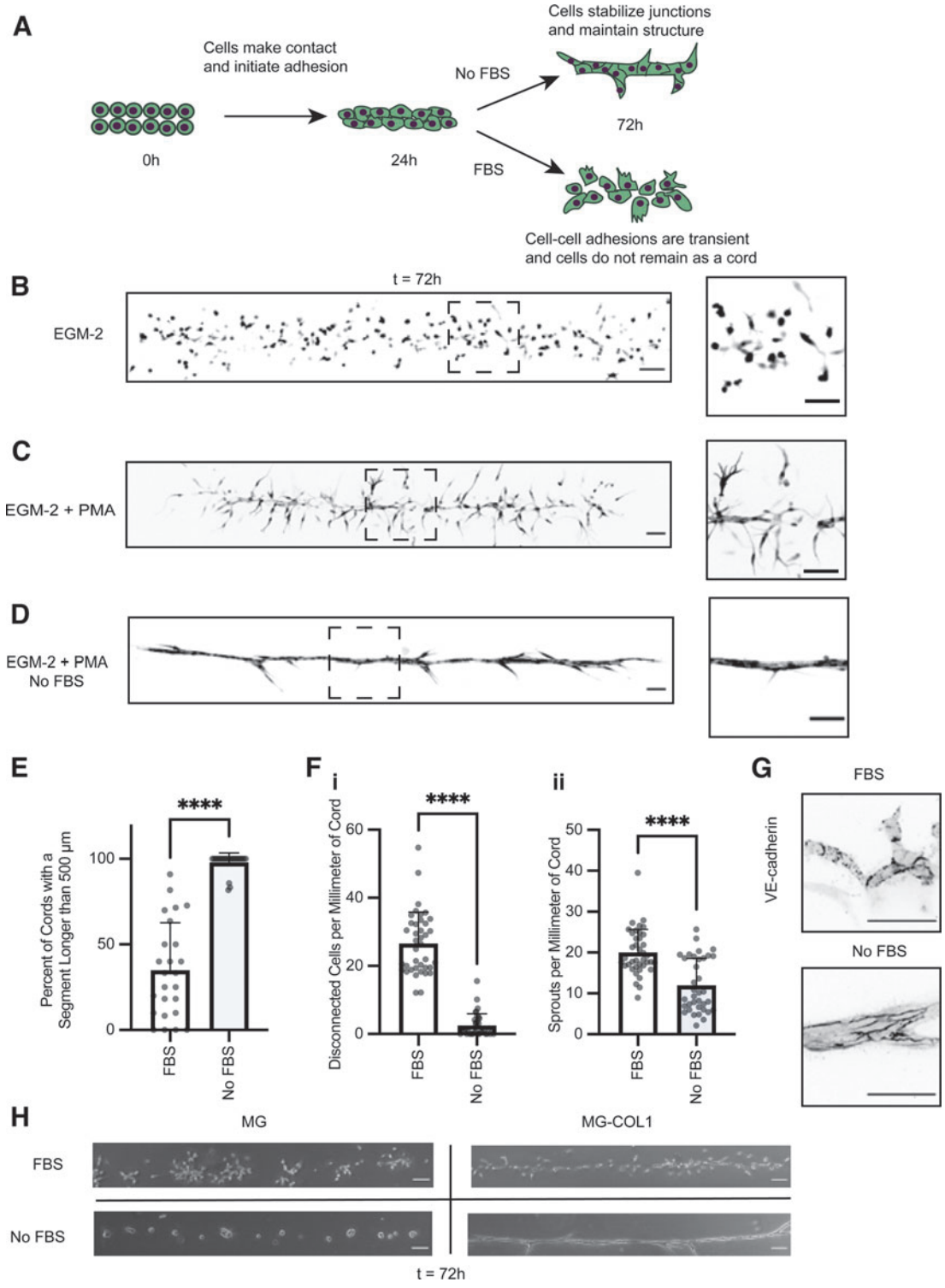

extended culture. Instead, we found that the cells scattered over the following 48 h (Fig. 2B). We hypothesized that EGM-2 media lacked factors necessary to maintain and stabilize cell–cell junctions. PMA has been previously shown to promote angiogenesis.[44–46] Addition of 50 ng/mL PMA modestly reduced HUVEC scattering and increased the length of cord segments (Fig. 2C and Supplementary Fig. S2A). The addition of proangiogenic, provasculogenic growth factors,[47–49] FGF-2, VEGF-A, and TGF-β, had no effect on cord morphology (Supplementary Fig. S2B). The combination of SDF-1α, IL-3, and SCF has been shown previously to promote vascular tube morphogenesis[48] but had no effect in this assay (Supplementary Fig. S2B).

The inability to stabilize cord morphology through added factors suggested an alternative hypothesis—that EGM-2 contained factors that antagonize cell behaviors necessary

for stable cord formation. FBS is a component of EGM-2 that contains many poorly characterized factors that could contribute to cell scattering.[50,51] Strikingly, omitting FBS, normally 2% of the volume of EGM-2, had a dramatic effect on cord morphology. Without FBS in the media, the HUVECs remained tightly adhered to one another and maintained the original patterned shape without scattering (Fig. 2D, E). There was also a reduction in the number of sprouts arising from the main cord (Fig. 2F). Staining for vascular endothelial-cadherin revealed that adherens junctions are impacted by FBS (Fig. 2G), having a ragged appearance at cell–cell junctions and exhibiting punctate staining within the cell, consistent with endocytosis and an angiogenic phenotype.[52,53]

These results suggest that FBS promotes the destabilization of adherens junctions and breakdown of endothelial cord structure. Combining these findings with the stabilizing influence of COL1-containing ECM, we concluded that matrices containing fibrillar collagen promote more extended morphologies than pure Matrigel and that factors within FBS destabilize a cord-like morphology (Fig. 2H).

FBS contains many beneficial components that support cell viability and growth.[50] We, therefore, sought to identify whether we could selectively remove the activity in FBS contributing to the scattering phenotype without omitting the beneficial components. Fractionation of the FBS using molecular weight cutoff filters demonstrated that the active component(s) of FBS had a molecular weight >200 kDa (Supplementary Fig. S3). The activity was present in heat-inactivated FBS, charcoal-stripped FBS, and exosome-depleted FBS, suggesting it was not part of the complement system, a lipophilic molecule, or an exosome, respectively. Proteinase K treatment of the FBS blocked its effects, suggesting that the active component of FBS contains a protein. We tested a range of candidate proteins that are known to be present in plasma or serum[51,54] (Supplementary Fig. S4) but none was sufficient to induce cell scattering from patterned cords when added to the media.

To better understand how the unidentified component in FBS was contributing to cord destabilization, we used live cell imaging to examine individual cellular behaviors within the patterned cord. In the presence of FBS, we observed ECs extending many protrusions, making transient adhesions with other ECs, and then migrating away from the main cord (Supplementary Video S1). In the absence of FBS, the ECs were elongated and moved back and forth along the cord but remained adhered to other ECs (Supplementary Video S2). To investigate these cell-cell interactions in greater detail, we used DPAC to pattern pairs of ECs separated by 25 μm as minimal ''tissues'' that were cultured in the presence and absence of FBS (Fig. 3A). Time-lapse microscopy revealed striking differences in morphology and cell behavior due to the media composition (Supplementary Videos S3, S4). EC pairs cultured with FBS had a star-shaped morphology, with protrusions extending in all directions. In contrast, EC pairs cultured in serum-free medium tended to elongate and had fewer protrusions (Fig. 3B).

FBS also resulted in more transient cell–cell adhesions, as measured by the average number of instances where the cells separated over the course of the time lapse (Fig. 3C). These observations further suggest that the active component in FBS destabilizes cords through its effects on cell–cell junctions and by promoting cell morphologies and patterns of motility that increase the probability of cells moving away from their nearest neighbors.

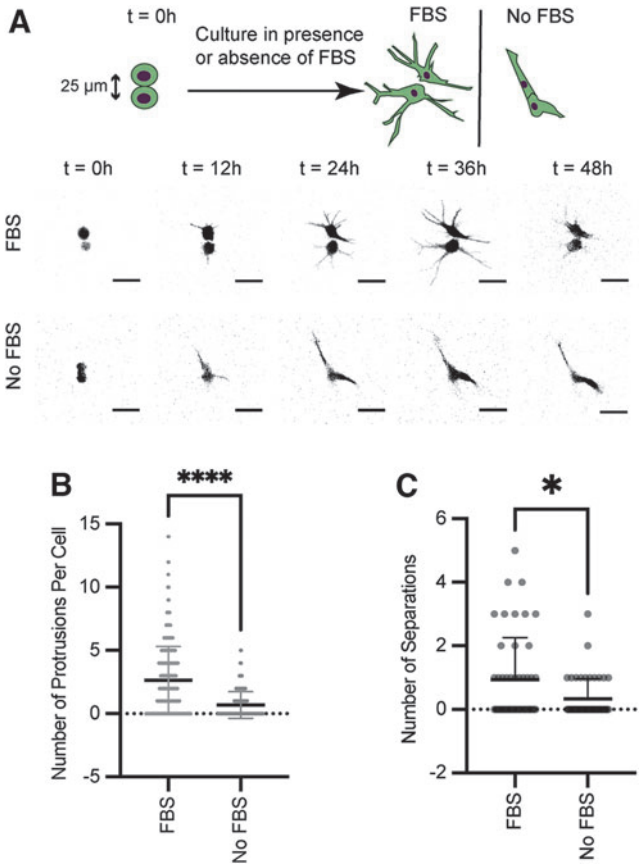

FIG. 3. FBS increases proliferation and extension of subcellular protrusions but inhibits the formation of stable cell–cell adhesions. **(A)** Pairs of HUVECs were patterned 25 μm apart (center to center distance) and cultured for 60 h in either FBS-free EGM-2 + PMA or FBS-containing EGM-2 + PMA. Cell pairs were imaged once per hour between hours 13–60. **(B)** Quantification of the number of protrusions per cell. Error bars represent the mean ± SD. Each data point represents one cell. Mann-Whitney U test, $p < 0.0001$. $n = 360$ cells for EGM-2 + PMA + FBS and $n = 199$ cells for EGM-2 + PMA without FBS. **(C)** Quantification of the average number of instances over the time lapse where the two cells in a pair lost contact with each other. Error bars represent the mean ± SD. Each data point represents one cell pair. Mann-Whitney U test, $p < 0.05$. $n = 48$ cell pairs for EGM-2 + PMA + FBS and $n = 46$ cell pairs for EGM-2 + PMA without FBS. $^{*}p < 0.05$, $^{****}p < 0.0001$.

Having identified microenvironmental conditions and cell behaviors that promote stable cord formation, we investigated how these structures progress through additional steps of microvascular self-organization (Fig. 4A). Endothelial cords cultured without FBS were stable and exhibited little change in cord morphology over 7 days (Fig. 4B) and could be cultured for at least 14 days (Supplementary Fig. S5). Staining for ZO-1 and claudin-5 revealed tight junctions between the ECs of these microvessels (Fig. 4C, D). The presence of an endothelial-derived basement membrane around the endothelial cords was confirmed by staining for human collagen IV (Fig. 4E).

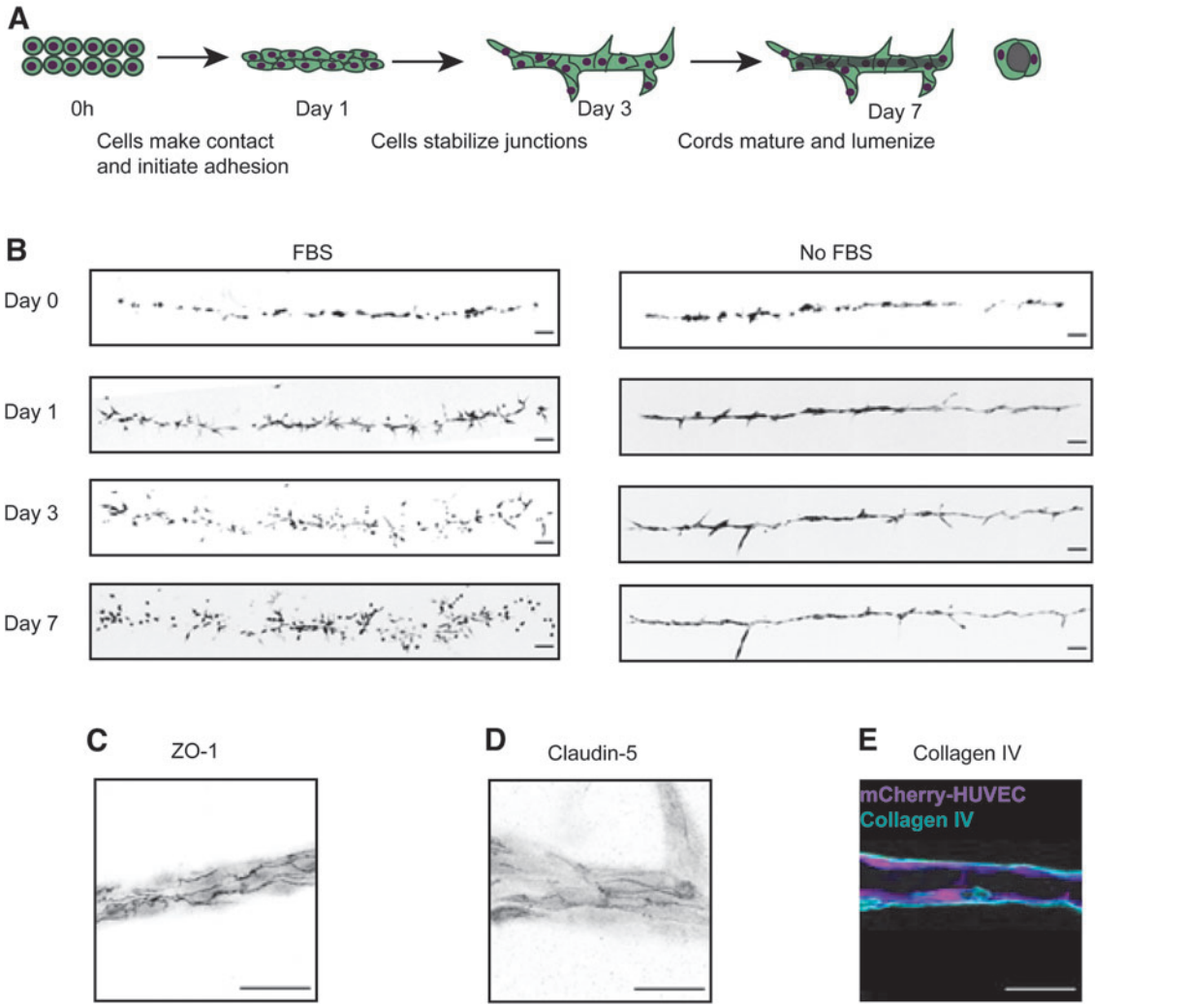

FIG. 4. Formation of stable, lumenized, and mature microvascular networks of controlled dimensions after extended culture of HUVEC cords in serum-free medium. **(A)** Diagram of the HUVEC cords progressing through the stages of vasculogenesis toward maturation and lumenization. **(B)** HUVEC cords were cultured in EGM-2 + PMA either containing or omitting FBS for 7 days. The same cords were imaged each time, demonstrating the extent of cord morphology change over time. Scale bar = 100 μm. **(C)** ZO-1 localized to the cell–cell junctions. Scale bar = 50 μm. **(D)** The endothelial tight junction protein claudin-5 was present at the cell–cell junctions. Scale bar = 50 μm. **(E)** HUVEC cords (*magenta*) were able to synthesize a basement membrane around themselves (collagen IV, *cyan*). Scale bar = 50 μm.

While cords appeared stable in this assay, we did not see clear evidence of lumenization—a final step in cord self-organization necessary for perfusion. Lumenization of blood vessels can occur through several different mechanisms.[55–57] We hypothesized that by increasing the cell–cell surface area, we could facilitate the formation of a lumen between ECs.[58] We patterned three-layered HUVEC cords that were 30–75 μm in diameter (Supplementary Fig. S6A, B) and condensed into a stable, continuous structure in serum-free medium (Supplementary Fig. S6C). However, we also

FIG. 5. Microenvironmental engineering of lumenized and perfusable microvasculature with defined vessel architecture. **(A)** Cell and nuclear debris (*white arrowheads*) observed in the center of a three-layered EGFP-EF1a (*green*), mScarlet-H2B (*magenta*) HUVEC cord after 5 days of culture in serum-free EGM-2. Scale bar = 500 μm. *Inset*: Closeup image of debris. Scale bar = 50 μm. **(B)** Microinjection of PBS into a three-layered microvessel resulted in the removal of cell debris, revealing an intact lumen down the length of the microvessel. **(C,** i) A three-layered mCherry-HUVEC microvessel (*magenta*) was perfused with 2 μm diameter blue fluorescent beads (*cyan*) (*white arrowheads*) Scale bar = 50 μm. (ii) The paths of beads were tracked over time, demonstrating fluid flow through the lumen. **(D)** A perfused cord was imaged with a confocal microscope, revealing an empty lumen surrounded by mCherry-HUVECs (*magenta*). Polarization is evident by actin (*cyan*) and laminin α5 (*yellow*) staining. Scale bar = 50 μm. **(E)** A three-layered mCherry-HUVEC cord (*magenta*) was cocultured with EGFP-HBVPs (*green*), leading to the deposition of a collagen IV-rich basement membrane (*cyan*). Scale bar = 50 μm. **(F)** A stylized branched microvascular network was created by patterning EGFP-HUVECs and culturing them in MG-COL1. Image taken after 19 h of culture. *Boxed region* shown in detail in panel G. **(G)** After 6 days of culture, the branched structure was perfused with a micropipette. The images show a progression of the debris being washed out of the lumen. Scale bar = 100 μm. PBS, phosphate buffered saline.

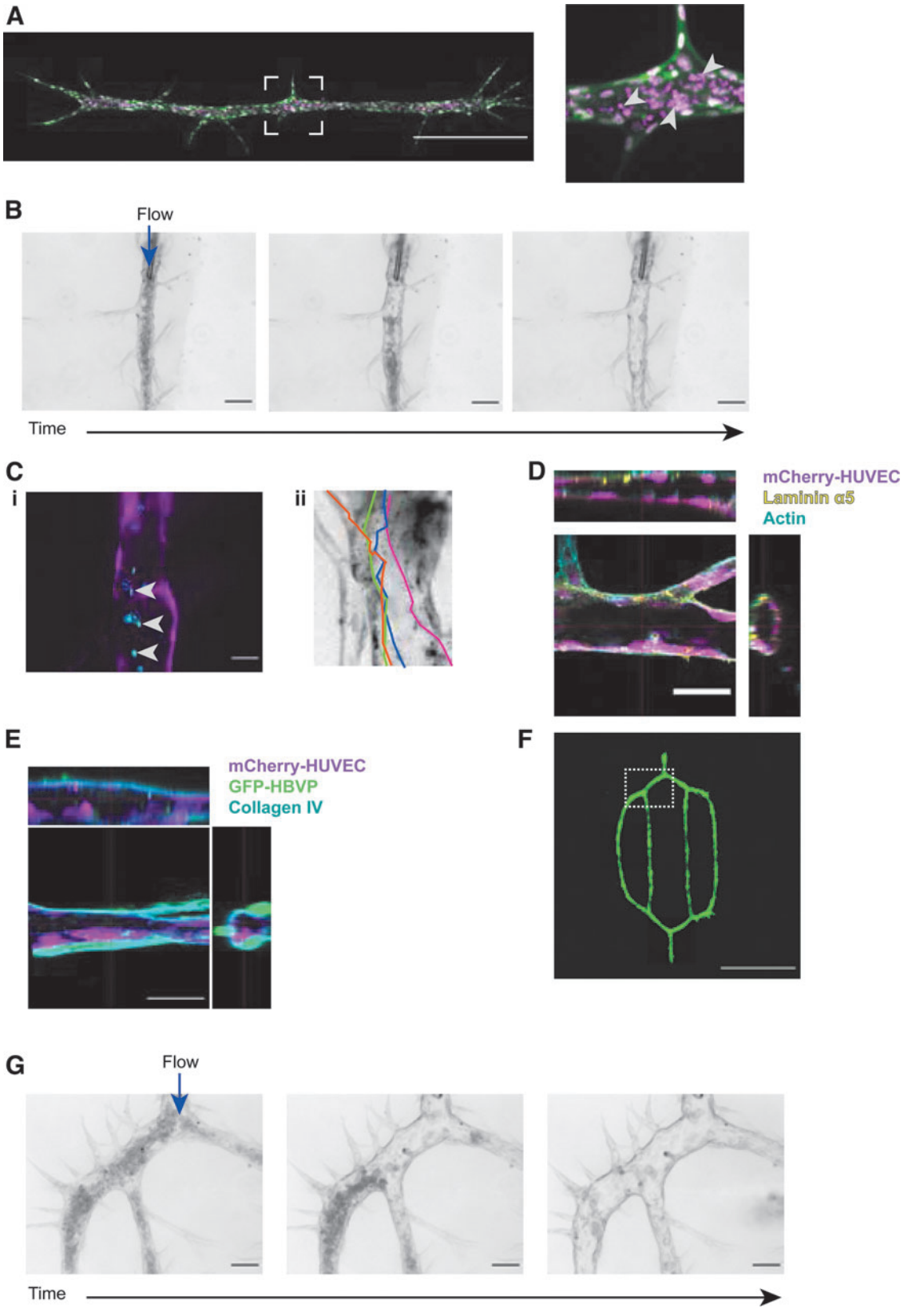
A
B
Flow
Time
C
i
ii
D
mCherry-HUVEC
Laminin α5
Actin
E
mCherry-HUVEC
GFP-HBVP
Collagen IV
F
G
Flow
Time

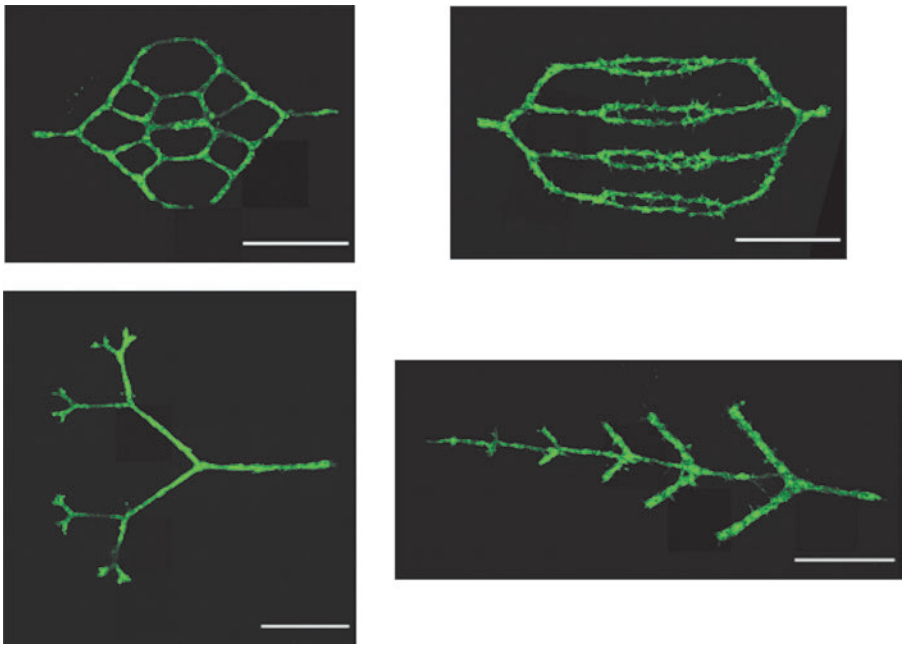

FIG. 6. Branched microvascular structures created using DPAC. Hierarchical, branched microvascular structures millimeters in length can be designed and engineered using DPAC with complete control over the final structure. Pictured here are patterned EGFP-HUVECs after 19 h of culture. Scale bar: 1000 μm.

observed cell debris accumulating in the center of these larger cords consistent with the onset of lumenization by cavitation[59] (Fig. 5A). We investigated whether these vessels were perfusable by cutting the vessel at one end and piercing the other end with a micropipette connected to a syringe. Upon injection of PBS, the cell debris was flushed through the cord, revealing a fully lumenized, perfusable microvessel (Fig. 5B and Supplementary Video S5).

Fluorescent microbeads injected into the lumen traveled the length of the vessel (Fig. 5C and Supplementary Video S6). The microvessels could be perfused within 3 days after patterning. Confocal imaging revealed an open lumen and a polarized endothelium with apical actin and basal laminin α5 (Fig. 5D). The cords exhibited endothelial barrier function for both small molecule dyes and fluorescently labeled proteins (Supplementary Fig. S7). When HBVPs were patterned on top of the ECs, they formed close associations with the ECs and were embedded within the vascular basement membrane (Fig. 5E). We created a variety of branched microvascular network structures with diameters ranging from 14 to 199 μm (Figs. 5F and 6), which could also be perfused across branch points (Fig. 5G and Supplementary Video S7). Thus, by engineering the microenvironment to control the process of vascular self-organization from patterned ECs, we were able to create mature and perfusable microvessels incorporating mural cells with a controlled branching architecture.

Discussion

Numerous studies have demonstrated efficient formation of microvessels through vasculogenesis, but control over the resulting network structures and vessel diameters is often lacking. We reasoned that tissue engineers could promote the maturation of prepatterned ECs into cords and vessels that retain fidelity to their designed pattern by considering the ''design principles'' of self-organization during vasculogenesis. Self-organization during traditional *in vitro* vasculogenesis assays involves a variety of EC behaviors that play specific roles during each stage of the process. ECs must first migrate, proliferate, and extend protrusions to establish contacts with other ECs, then switch to a different set of cell behaviors that promote maturation by stabilizing nascent cell–cell adhesions, polarizing, and lumenizing.

By using high-resolution cell patterning to place the ECs adjacent to each other, the process effectively starts at the midway point, reducing the cell behaviors necessary for efficient self-organization. We used DPAC to test this idea by patterning ECs in cords of similar diameter and cell density to capillaries. These cords provided us with a reliable assay to test the effects of microenvironmental cues necessary for self-organization of patterned ECs into mature perfusable microvessels.

Endothelial cord formation requires that initially close-packed cells stabilize cell–cell interfaces while maintaining an extended geometry on their basal interface. This process requires reorganization of the contractile apparatus at cell–cell and cell–ECM interfaces, and therefore requires a substrate capable of sustaining the resulting active tensions generated by the cells. We found that matrix composition is critical for this process. Patterned HUVEC cords cultured in Matrigel were unable to maintain an extended and cohesive structure. Instead, the patterned lines of cells broke up into several smaller cohesive clusters, or ''droplets,'' consistent with a high interfacial tension between the basal surface of the ECs and the surrounding gel.[60,61] We hypothesized that to balance their interfacial tension at the basal surface, the cells required a fibrous component of the ECM, which can be organized into a more mechanically stable substrate. This concept plays an important role in the morphogenesis of a variety of tissues.[42] Indeed, we found that fluorescently labeled matrix was concentrated at the basal surface of HUVEC cords cultured in MG-COL1 through a process known to involve cell contractility.[15,42]

After the formation of cell–cell and cell–ECM interfaces, the microenvironment must provide signals supporting the maintenance of those interfaces while removing signals that promote interface turnover.[62] However, we found that groups

of ECs cultured in Matrigel and collagen I disbanded into individual ECs after 72 h of culture. We explored the addition of media factors previously described to promote cord formation through randomly seeded vasculogenesis or angiogenesis (e.g., VEGF, FGF).[48] Surprisingly, these conditions did not enhance cord stability when the cells were seeded directly into a cord-like geometry. A potential explanation for this observation is that proangiogenic factors are useful when tip cell-like behaviors, such as migration and extension of protrusions are desired.[63,64] However, when cell behaviors promoting microvessel stabilization and maturation are required, these factors provided no additional benefit and may in fact oppose microvessel stability. We reasoned a subset of factors present in FBS were promoting tip cell-associated behaviors, leading to destabilization of cell–cell interfaces.

Careful examination of the underlying cell behaviors promoted by FBS revealed the extension of protrusions and a decreased lifetime of cell–cell interfaces, both behaviors associated with angiogenic tip cells but not stable microvasculature.[65,66] Removal of a high-molecular-weight and protein-based component of FBS allowed the engineering of stable, branched, and perfusable vascular networks. Thus, both the mechanical and chemical components of the microenvironment must be tailored to promote the specific cell behaviors necessary for the self-organization of prepatterned tissues—behaviors that might be opposed by factors necessary for cell expansion and migration. In this study, we largely focused on ECs alone, but future studies that integrate multiple vascular and parenchymal cell types will have to identify microenvironmental conditions that promote the ideal cell behaviors for each and every cell type in the tissue.

An important limitation of this study is that the vessels were not continuously perfused during culture and were only perfusable after being pierced with a micropipette. Continuous perfusion might have further facilitated lumen formation,[67] prevented the buildup of luminal debris, and aided maturation and quiescence.[68,69] DPAC imposes several engineering constraints onto a potential microfluidic perfusion system, including the need to sandwich multiple layers of hydrogel and PDMS while remaining watertight. However, the flexibility, scalability, and high resolution of DPAC allowed us to create microvessels of diverse shapes and sizes, including capillary-sized microvessels (diameter $\sim 10\,\mu m$) and branched vascular networks, millimeters in length. The microenvironmental engineering principles identified in this study should be applicable to other advanced methods for engineering microvasculature, which may be more amenable to perfusion at earlier time points. For example, the microenvironmental cues identified in this article could be applied to further promote the rapid self-organization of ECs patterned through extrusion bioprinting.[3]

The strategies explored in this study could also be used to engineer narrower gauge vessels that interface with larger vessels prepared using biofabrication methods, such as laser ablation[25] or the bioprinting of sacrificial materials[20,70] that create endothelial-lined channels hundreds of microns in diameter. By combining fabrication methods, one could create an engineered tissue that is initially perfused with larger endothelial-lined channels but includes densely patterned ECs branching from these channels. Over a few days, the patterned ECs could self-organize into microvessels that anastomose with the channels. This approach would combine the advantages of DPAC (microvascular resolution, complete control over structure) with the scalability and perfusability of top–down biofabrication methods.

Authors' Contributions

K.A.C., V.S., A.J.G., and C.S. performed experiments. M.C.C. helped to develop the methodology and contributed to the article's ideas. Z.J.G. and V.W. supervised experiments. K.A.C. and Z.J.G. wrote the article with feedback and approval from all authors.

Disclosure Statement

Z.J.G. is an equity holder in Scribe Biosciences and Provenance Bio. K.A.C. is an equity holder in GC Therapeutics.

Funding Information

This research was supported in part by grants from the Department of Defense Breast Cancer Research Program (W81XWH-10-1-1023 and W81XWH-13-1-0221), NIH (U01CA199315, DP2 HD080351-01, 1R01CA190843-01, 1R21EB019181-01A, and 1R21CA182375-01A1), the NSF (MCB1330864), and the UCSF Center for Cellular Construction (DBI-1548297), an NSF Science and Technology Center. Z.J.G is a Chan-Zuckerberg BioHub Investigator. Sorting of fluorescent cells was done in the UCSF Laboratory for Cell Analysis, a core facility supported by a National Cancer Institute Cancer Center Support Grant (P30CA082103). Viruses were produced in the Viracore at UCSF.

Supplementary Material

Supplementary Methods
Supplementary Figure S1
Supplementary Figure S2
Supplementary Figure S3
Supplementary Figure S4
Supplementary Figure S5
Supplementary Figure S6
Supplementary Figure S7
Supplementary Video S1
Supplementary Video S2
Supplementary Video S3
Supplementary Video S4
Supplementary Video S5
Supplementary Video S6
Supplementary Video S7

References

1. Laurent J, Blin G, Chatelain F, et al. Convergence of microengineering and cellular self-organization towards functional tissue manufacturing. Nat Biomed Eng 2017;1(12):939–956; doi: 10.1038/s41551-017-0166-x
2. Brassard JA, Lutolf MP. Engineering stem cell self-organization to build better organoids. Cell Stem Cell 2019;24(6):860–876; doi: 10.1016/j.stem.2019.05.005
3. Brassard JA, Nikolaev M, Hübscher T, et al. Recapitulating macro-scale tissue self-organization through organoid bioprinting. Nat Mater 2020;20:22–29; doi: 10.1038/s41563-020-00803-5
4. Morgan JT, Shirazi J, Comber EM, et al. Fabrication of centimeter-scale and geometrically arbitrary vascular net-

works using in vitro self-assembly. Biomaterials 2018;189(October 2018):37–47; doi: 10.1016/j.biomaterials.2018.10.021
5. Whisler JA, Chen MB, Kamm RD. Control of perfusable microvascular network morphology using a multiculture microfluidic system. Tissue Eng Part C Methods 2013;20(7):1–38; 10.1089/ten.TEC.2013.0370
6. Bogorad MI, DeStefano J, Karlsson J, et al. Review: In vitro microvessel models. Lab Chip 2015;15(22):4242–4255; doi: 10.1039/C5LC00832H
7. Davis GE, Bayless KJ, Mavila A. Molecular basis of endothelial cell morphogenesis in three-dimensional extracellular matrices. Anat Rec 2002;268(3):252–275; doi: 10.1002/ar.10159
8. Collinet C, Lecuit T. Programmed and self-organized flow of information during morphogenesis. Nat Rev Mol Cell Biol 2021;22(4):245–265; doi: 10.1038/s41580-020-00318-6
9. Song HHG, Rumma RT, Ozaki CK, et al. Vascular tissue engineering: Progress, challenges, and clinical promise. Cell Stem Cell 2018;22(3):340–354; doi: 10.1016/j.stem.2018.02.009
10. McLeod C, Higgins J, Miroshnikova Y, et al. Microscopic matrix remodeling precedes endothelial morphological changes during capillary morphogenesis. J Biomech Eng 2013;135(7):71002; doi: 10.1115/1.4023984
11. Rao RR, Peterson AW, Ceccarelli J, et al. Matrix composition regulates three-dimensional network formation by endothelial cells and mesenchymal stem cells in collagen/fibrin materials. Angiogenesis 2012;15(2):253–264; doi: 10.1007/s10456-012-9257-1
12. Moya ML, Hsu Y-H, Lee AP, et al. In vitro perfused human capillary networks. Tissue Eng Part C Methods 2013;19(9):730–737; doi: abs/10.1089/ten.tec.2012.0430
13. Kim S, Lee H, Chung M, et al. Engineering of functional, perfusable 3D microvascular networks on a chip. Lab Chip 2013;13:1489–1500; doi: 10.1039/C3LC41320A
14. Rajasekar S, Lin DSY, Abdul L, et al. IFlowPlate—A customized 384-well plate for the culture of perfusable vascularized colon organoids. Adv Mater 2020;32(46):1–12; doi: 10.1002/adma.202002974
15. Utzinger U, Baggett B, Weiss JA, et al. Large-scale time series microscopy of neovessel growth during angiogenesis. Angiogenesis 2015;18:219–232; doi: 10.1007/s10456-015-9461-x
16. Murray CD. The physiological principle of minimum work applied to the angle of branching of arteries. J Gen Physiol 1926;9(6):835–841; doi: 10.1085/jgp.9.6.835
17. White S, Pittman C, Hingorani R, et al. Implanted cell-dense prevascularized tissues develop functional vasculature that supports reoxygenation following thrombosis. Tissue Eng Part A 2014;20(17–18):2316–2328; doi: 10.1089/ten.TEA.2013.0311
18. Folkman J, Hochberg M. Self-regulation of growth in three dimensions. J Exp Med 1973;138(4):745–753; doi: 10.1084/jem.138.4.745
19. Griffith CK, Miller C, Sainson RC, et al. Diffusion limits of an in vitro thick prevascularized tissue. Tissue Eng 2005;11(1–2):257–266; doi: 10.1089/ten.2005.11.257
20. Miller JS, Stevens KR, Yang MT, et al. Rapid casting of patterned vascular networks for perfusable engineered three-dimensional tissues. Nat Mater 2012;11:768–774; doi: 10.1038/nmat3357
21. Polacheck WJ, Kutys ML, et al. Microfabricated blood vessels for modeling the vascular transport barrier. Nat Protoc 2019;14(5):1425–1454; doi: 10.1038/s41596-019-0144-8
22. Zheng Y, Chen J, Craven M, et al. In vitro microvessels for the study of angiogenesis and thrombosis. Proc Natl Acad Sci U S A 2012;109(24):9342–9347; doi: 10.1073/pnas.1201240109
23. Grigoryan B, Paulsen SJ, Corbett DC, et al. Multivascular networks and functional intravascular topologies within biocompatible hydrogels. Science 2019;364(6439):458–464; doi: 10.1126/science.aav9750
24. Heintz KA, Bregenzer ME, Mantle JL, et al. Fabrication of 3D biomimetic microfluidic networks in hydrogels. Adv Healthc Mater 2016;5(17):2153–2160; doi: 10.1002/adhm.201600351
25. Rayner SG, Howard CC, Mandrycky CJ, et al. Multiphoton-guided creation of complex organ-specific microvasculature. Adv Healthc Mater 2021;2100031:2100031; doi: 10.1002/adhm.202100031
26. Chrobak KM, Potter DR, Tien J. Formation of perfused, functional microvascular tubes in vitro. Microvasc Res 2006;71:185–196; doi: 10.1016/j.mvr.2006.02.005
27. Reid JA, Mollica PM, Bruno RD, et al. Consistent and reproducible cultures of large-scale 3D mammary epithelial structures using an accessible bioprinting platform. Breast Cancer Res 2018;1–13; doi: 10.1186/s13058-018-1045-4
28. Malheiro A, Wieringa P, Mota C, et al. Patterning vasculature: The role of biofabrication to achieve an integrated multicellular ecosystem. ACS Biomater Sci Eng 2016;2(10):1694–1709; doi: 10.1021/acsbiomaterials.6b00269
29. Hoch E, Tovar GEM, Borchers K. Bioprinting of artificial blood vessels: Current approaches towards a demanding goal. Eur J Cardiothorac Surg 2014;46(June):1–12; doi: 10.1093/ejcts/ezu242
30. Todhunter ME, Jee NY, Hughes AJ, et al. Programmed synthesis of three-dimensional tissues. Nat Methods 2015;12(10):975–981; doi: 10.1038/nmeth.3553
31. Todhunter ME, Weber RJ, Farlow J, et al. Fabrication of 3D microtissue arrays by DNA programmed assembly of cells. Curr Protoc Chem Biol 2016;8(3):147–178; doi: 10.1002/cpch.8
32. Cabral KA, Patterson DM, Scheideler OJ, et al. Simple, affordable, and modular patterning of cells using DNA. J Vis Exp 2021;(168); doi: 10.3791/61937
33. Scheideler OJ, Yang C, Kozminsky M, et al. Recapitulating complex biological signaling environments using a multiplexed, DNA-patterning approach. Sci Adv 2020;6(12):eaay5696; doi: 10.1126/sciadv.aay5696
34. Schindelin J, Arganda-Carreras I, Frise E, et al. Fiji: An open-source platform for biological-image analysis. Nat Methods 2012;9(7):676–682; doi: 10.1038/nmeth.2019
35. Adamson RH. Microvascular endothelial cell shape and size in situ. Microvasc Res 1993;46:77–88; doi: 10.1006/mvre.1993.1036
36. Lancaster MA, Corsini NS, Wolfinger S, et al. Guided self-organization and cortical plate formation in human brain organoids. Nat Biotechnol 2017;35(7):659–666; doi: 10.1038/nbt.3906
37. Sato T, Vries RG, Snippert HJ, et al. Single Lgr5 stem cells build crypt-villus structures in vitro without a mesenchymal niche. Nature 2009;459(7244):262–265; doi: 10.1038/nature07935
38. Jamieson PR, Dekkers JF, Rios AC, et al. Derivation of a robust mouse mammary organoid system for studying tissue dynamics. Development 2016;144(6):1065–1071; doi: 10.1242/dev.145045
39. Yeung T, Georges PC, Flanagan LA, et al. Effects of substrate stiffness on cell morphology, cytoskeletal structure, and adhesion. Cell Motil Cytoskeleton 2005;60(1):24–34; doi: 10.1002/cm.20041

40. Mason BN, Starchenko A, Williams RM, et al. Tuning three-dimensional collagen matrix stiffness independently of collagen concentration modulates endothelial cell behavior. Acta Biomater 2013;9(1):4635–4644; doi: 10.1016/j.actbio.2012.08.007
41. Hughes AJ, Miyazaki H, Coyle MC, et al. Engineered tissue folding by mechanical compaction of the mesenchyme. Dev Cell 2018;44(2):165–178.e6; doi: 10.1016/j.devcel.2017.12.004
42. Buchmann B, Engelbrecht LK, Fernandez P, et al. Mechanical plasticity of collagen directs branch elongation in human mammary gland organoids. Nat Commun 2021;12(1):2759; doi: 10.1038/s41467-021-22988-2
43. Ban E, Franklin JM, Nam S, et al. Mechanisms of plastic deformation in collagen networks induced by cellular forces. Biophys J 2018;114(2):450–461; doi: 10.1016/j.bpj.2017.11.3739
44. Nishizuka Y. The role of protein kinase C in cell surface signal transduction and tumour promotion. Nature 1984;308(5961):693–698; doi: 10.1038/308693a0
45. Montesano R, Orci L. Tumor-promoting phorbol esters induce angiogenesis in vitro. Cell 1985;43:469–477; doi: 10.1016/0092-8674(85)90104-7
46. Nguyen D-HT, Stapleton SC, Yang MT, et al. Biomimetic model to reconstitute angiogenic sprouting morphogenesis in vitro. Proc Natl Acad Sci U S A 2013;110(17):6712–6717; doi: 10.1073/pnas.1221526110
47. Koch S, Tugues S, Li X, et al. Signal transduction by vascular endothelial growth factor receptors. Biochem J 2011;437(2):169–183; doi: 10.1042/BJ20110301
48. Stratman AN, Davis MJ, Davis GE. VEGF and FGF prime vascular tube morphogenesis and sprouting directed by hematopoietic stem cell cytokines. Blood 2011;117(14):3709–3719; doi: 10.1182/blood-2010-11-316752
49. Patel-Hett S, D'Amore PA. Signal transduction in vasculogenesis and developmental angiogenesis. Int J Dev Biol 2011;55(4–5):353–363; doi: 10.1387/ijdb.103213sp
50. Yao T, Asayama Y. Animal-cell culture media: History, characteristics, and current issues. Reprod Med Biol 2017;16(2):99–117; doi: 10.1002/rmb2.12024
51. Anderson NL, Anderson NG. The human plasma proteome. Mol Cell Proteomics 2002;1(11):845–867; doi: 10.1074/mcp.R200007-MCP200
52. Gavard J, Gutkind JS. VEGF controls endothelial-cell permeability by promoting the β-arrestin-dependent endocytosis of VE-cadherin. Nat Cell Biol2006;8(11):1223–1234; doi: 10.1038/ncb1486
53. Bentley K, Franco CA, Philippides A, et al. The role of differential VE-cadherin dynamics in cell rearrangement during angiogenesis. Nat Cell Biol 2014;16(4):309–321; doi: 10.1038/ncb2926
54. Zheng X, Baker H, Hancock WS, et al. Proteomic analysis for the assessment of different lots of fetal bovine serum as a raw material for cell culture. Part IV. Application of proteomics to the manufacture of biological drugs. Biotechnol Prog 2006;22(5):1294–1300; doi: 10.1021/bp060121o
55. Lammert E, Axnick J. Vascular lumen formation. Cold Spring Harb Perspect Med 2012;2(4):a006619; doi: 10.1101/cshperspect.a006619
56. Zeeb M, Strilic B, Lammert E. Resolving cell-cell junctions: Lumen formation in blood vessels. Curr Opin Cell Biol 2010;22(5):626–632; doi: 10.1016/j.ceb.2010.07.003
57. Xu K, Cleaver O. Tubulogenesis during blood vessel formation. Semin Cell Dev Biol 2011;22(9):993–1004; doi: 10.1016/j.semcdb.2011.05.001
58. Strilić B, Eglinger J, Krieg M, et al. Electrostatic cell-surface repulsion initiates lumen formation in developing blood vessels. Curr Biol 2010;20(22):2003–2009; doi: 10.1016/j.cub.2010.09.061
59. Sigurbjörnsdóttir S, Mathew R, Leptin M. Molecular mechanisms of de novo lumen formation. Nat Rev Mol Cell Biol 2014;15(10):665–676; doi: 0.1038/nrm3871
60. Brodland GW. The Differential Interfacial Tension Hypothesis (DITH): A comprehensive theory for the self-rearrangement of embryonic cells and tissues. J Biomech Eng 2002;124(2):188–197; doi: 10.1115/1.1449491
61. Morley CD, Ellison ST, Bhattacharjee T, et al. Quantitative characterization of 3D bioprinted structural elements under cell generated forces. Nat Commun 2019;10(1):1–9; doi: 10.1038/s41467-019-10919-1
62. Nerger BA, Siedlik MJ, Nelson CM. Microfabricated tissues for investigating traction forces involved in cell migration and tissue morphogenesis. Cell Mol Life Sci 2017;74(10):1819–1834; doi: 10.1007/s00018-016-2439-z
63. Betz C, Lenard A, Belting H, et al. Cell behaviors and dynamics during angiogenesis. Development 2016;143(13):2249–2260; doi: 10.1242/dev.135616
64. Gerhardt H, Golding M, Fruttiger M, et al. VEGF guides angiogenic sprouting utilizing endothelial tip cell filopodia. J Cell Biol 2003;161(6):1163–1177; doi: 10.1083/jcb.200302047
65. Szymborska A, Gerhardt H. Hold me, but not too tight—Endothelial cell–cell junctions in angiogenesis. Cold Spring Harb Perspect Biol 2018;10(8):a029223; doi: 10.1101/cshperspect.a029223
66. Tung JJ, Tattersall IW, Kitajewski J. Tips, stalks, tubes: Notch-mediated cell fate determination and mechanisms of tubulogenesis during angiogenesis. Cold Spring Harb Perspect Med 2013;2(2):1–14; doi: 10.1101/cshperspect.a006601
67. Abe Y, Watanabe M, Chung S, et al. Balance of interstitial flow magnitude and vascular endothelial growth factor concentration modulates three-dimensional microvascular network formation. APL Bioeng 2019;3(3):036102; doi: 10.1063/1.5094735
68. Baeyens N, Nicoli S, Coon BG, et al. Vascular remodeling is governed by a VEGFR3-dependent fluid shear stress set point. Elife 2015;4:1–16; doi: 10.7554/eLife.04645
69. Baeyens N, Schwartz MA. Biomechanics of vascular mechanosensation and remodeling. Mol Biol Cell 2016;27(1):7–11; doi: 10.1091/mbc.E14-11-1522
70. Kinstlinger IS, Saxton SH, Calderon GA, et al. Generation of model tissues with dendritic vascular networks via sacrificial laser-sintered carbohydrate templates. Nat Biomed Eng 2020; doi: 10.1038/s41551-020-0566-1

Address correspondence to:
Zev J. Gartner, PhD
Department of Pharmaceutical Chemistry
University of California, San Francisco
N512E Genentech Hall, 600 16th Street
San Francisco, CA, 94158
USA

E-mail: zev.gartner@ucsf.edu

Received: April 1, 2022
Accepted: September 15, 2022
Online Publication Date: February 14, 2023